www.advanced-bio.com

CellMag-CARWash: A High Throughput Droplet Microfluidic Device for Live Cell Isolation and Single Cell Applications

Brittany T. Rupp, Claire D. Cook, Emma A. Purcell, Matei Pop, Abigail E. Radomski, Nicolas Mesyngier, Ryan C. Bailey,* and Sunitha Nagrath*

The recent push toward understanding an individual cell's behavior and identifying cellular heterogeneity has created an unmet need for technologies that can probe live cells at the single-cell level. Cells within a population are known to exhibit heterogeneous responses to environmental cues. These differences can lead to varied cellular states, behavior, and responses to therapeutics. Techniques are needed that are not only capable of processing and analyzing cellular populations at the single cell level, but also have the ability to isolate specific cell populations from a complex sample at high throughputs. The new CellMag-Coalesce-Attract-Resegment Wash (CellMag-CARWash) system combines positive magnetic selection with droplet microfluidic devices to isolate cells of interest from a mixture with >93% purity and incorporate treatments within individual droplets to observe single cell biological responses. This workflow is shown to be capable of probing the single cell extracellular vesicle (EV) secretion of MCF7 GFP cells. This article reports the first measurement of β -Estradiol's effect on EV secretion from MCF7 cells at the single cell level. Single cell processing revealed that MCF7 GFP cells possess a heterogeneous response to β -Estradiol stimulation with a 1.8-fold increase relative to the control.

1. Introduction

It has been established that within any population of seemingly identical cells, some cell-to-cell differences exist. $^{[1]}$ Traditional bulk analysis of a cell population often results in an average signal

of the population being reported, ignoring rare cell populations and heterogeneity within samples. Therefore, single cell studies have gained momentum over the past ten years as researchers have begun to recognize the value of being able to observe heterogeneity within cell populations.[2-6] Single cell sequencing and single cell multimodal omics enable high throughput analysis of many single cells.[7,8] Due to this, single cell functional studies are evolving. Studies examining heterogeneity in diseases such as cancer show how cellular differences can affect properties including immune response and drug resistance, among others.[9-11] Cells also demonstrate heterogeneity in their ability to signal and communicate with other cells, through either direct interactions or from secreting signaling molecules such as cytokines and extracellular vesicles (EVs).[12-15] Cell communication affects many important processes including cell development, growth,

differentiation, migration, and apoptosis.^[16–18] Single cell studies examining heterogeneity and how it relates to cellular behavior and function require the investigation of tens of thousands of cells for findings to significantly cover the breadth of possible cell states.^[19–21] Thus, there is a need for easy-to-use, affordable,

B. T. Rupp, E. A. Purcell, A. E. Radomski, S. Nagrath Department of Chemical Engineering University of Michigan Ann Arbor, MI 48109, USA E-mail: snagrath@umich.edu

B. T. Rupp, E. A. Purcell, M. Pop, S. Nagrath Biointerfaces Institute University of Michigan Ann Arbor, MI 48 109, USA

The ORCID identification number(s) for the author(s) of this article can be found under https://doi.org/10.1002/adbi.202400066

© 2024 The Authors. Advanced Biology published by Wiley-VCH GmbH. This is an open access article under the terms of the Creative Commons Attribution License, which permits use, distribution and reproduction in any medium, provided the original work is properly cited.

DOI: 10.1002/adbi.202400066

C. D. Cook, R. C. Bailey Department of Chemistry University of Michigan Ann Arbor, MI 48109, USA E-mail: ryancb@umich.edu

Ann Arbor, MI 48109, USA

Department of Biomedical Engineering University of Michigan Ann Arbor, MI 48109, USA

N. Mesyngier Department of Mechanical Engineering University of Michigan Ann Arbor, MI 48 109, USA S. Nagrath Rogel Cancer Center University of Michigan

ADVANCED BIOLOGY

www.advancedsciencenews.com

www.advanced-bio.com

integrated technologies that first perform high-throughput isolation of single cells for further manipulation and analysis.

The most common single cell isolation techniques are fluorescence activated cell sorting (FACS), magnetic-activated cell sorting (MACS), manual cell picking, and microfluidics. [22,23] FACS, MACS, and manual cell picking offer the ability to isolate single cells, but require large sample volumes, can be expensive, lack specificity, and/or require specialized training to perform. Alternatively, microfluidic technologies for single cell isolation are becoming increasingly common due to the ability to miniaturize assays.^[24] The small scale of microfluidic devices allows researchers to manipulate very small volumes of fluids, allowing them to minimize assay volumes. Commercial single-cell microfluidic technologies are available, including the DEPArray (DiElectroPhoresis Array), [25] which manipulates single cells in a chamber using dielectrophoresis, and integrated fluidic circuits (IFC) which moves single cells into chambers using a system of pressure-controlled microfluidic valves.^[26] Both technologies have been used in multiple studies to obtain single cell data, [27,28] but they suffer from limitations, such as lengthy processing time, lack of validation for use in live cells (DEPArray), and the ability to only collect a limited number of cells (IFC). [29,30]

Droplet-based microfluidics can enable compartmentalization and analysis of analytes in a high throughput fashion. Specifically, single cells can be isolated into single droplets surrounded by an immiscible oil phase, and, importantly for our work, the small volume droplet serves as a reaction chamber into which molecules and complexes secreted by encapsulated cells can be trapped for downstream analysis. Additionally, droplet microfluidic technologies are scalable,[24,31] allowing users to adjust the number of cells analyzed per experiment by modulating the volume emulsified. One successful commercially available single cell droplet microfluidic technology, the 10X Genomics Chromium system, has been used across multiple studies to examine chromatin accessibility, gene expression, and protein expression.^[32,33] However, for samples with contaminating cell populations, the Chromium system provides no pre-sorting of the sample to remove unwanted cells, necessitating either incorporation of an additional isolation step using techniques such as FACS, or removal of those cell populations during data analysis. Hence, there is a highly significant, unmet need for easy-to-use, streamlined strategies that can separate target cells from heterogeneous, complex samples and then interrogate them individually at the single cell level.

Here, we describe the adaptation and expansion of the droplet microfluidic Coalesce-Attract-Resegment Wash (CAR-Wash) system to isolate single target cells from a bulk cell mixture. The CAR-Wash system was originally developed to enrich small molecules attached to magnetic beads, such as proteins, by pulling the beads through immiscible phase boundaries to wash the contents attached to beads before resuspending them into product droplets.^[34] To expand the capabilities of the CAR-Wash, and overcome the limitations of higher drag forces on larger molecules and particles, alterations of parameters such as extending the washing chamber length, increasing the applied magnetic field, or lowering fluid flow rates would be needed. In this study, we demonstrate that the device can be utilized to isolate a specific cell population using antibody-tagged magnetic beads, which we term CellMag-CARWash. This was achieved by changing the de-

sign to feature a longer washing chamber than the original device. The efficiency and purity of this system was quantified on two different mixed populations of cells with different target antigens and was found to be high. Importantly, following isolation, cells are re-encapsulated into droplets, facilitating further downstream analysis at the single cell level.

While single cell droplet suspensions could be used for a variety of applications, such as single cell sequencing, we chose to demonstrate the utility of this isolation and re-encapsulation approach by studying EV secretion from live single cells. Specifically, there is very little known about the differences in EV secretion between individual cells as most methods of analysis are bulk methods, where EVs from many cells are pooled together. It is well-established that single cells can have variable secretion of molecules such as cytokines, and therefore, we hypothesized that EVs might be secreted at different levels by individual cells. However, bulk methods of EV collection and analysis would obscure this heterogeneity. Previous work on single cell EV secretion has been limited and involved either antibody-based capture of secreted EVs, which may miss EVs lacking expression of certain proteins, or culturing single cells in droplets to accumulate all EVs for quantification. Additionally, these single cell droplet microfluidic techniques required pure populations of cells as an input for droplet generation. [35,36] Therefore, in this study we employ the CellMag-CARWash system to selectively enrich a specific cell population from a mixture followed by an analysis of EV secretion from isolated, single cells. New insights into EV secretion at the single-cell level will expand our understanding of cell-tocell differences in response to stimuli, which will ground investigations into new diagnostic and therapeutic opportunities.

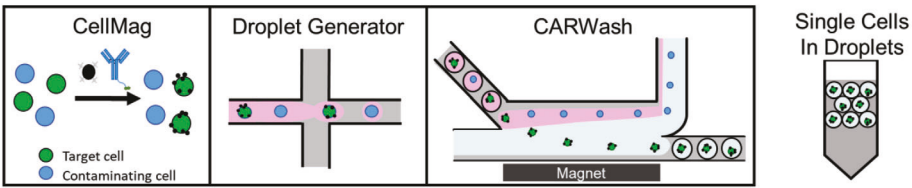
2. Results

The overall workflow of single cell isolation and EV secretion analysis is shown in Figure 1. Cells of interest within a complex mixture of multiple cell types were first tagged with specific, antibody-coated, magnetic beads (CellMag) and then suspended into droplets to distribute cells evenly throughout the solution volume and prevent settling due to gravity. Cells were then isolated via magnetophoretic separation through a stream of washing buffer and resuspended in new droplets in a continuous process (CARWash). Isolated single cells were incubated in suspension during which time EVs were secreted. Finally, EV analysis was achieved using a magnetic droplet splitter to remove beadtagged cells from the EV-containing single-cell supernatants and imaging droplets containing only EVs.

2.1. Attachment of Magnetic Beads to Cells Using Target Specific Antibodies

To test the CellMag-CARWash system, two samples composed of mixed cell populations were made: a mixture of Natural Killer 92mi (NK) and Jurkat T cells to examine the isolation of specific immune cells, and a mixture of MCF7 GFP and NK cells to examine the isolation of cancer cells from immune cells. The target cell populations were isolated through recognition of surface antigens by specific biotinylated antibodies coated onto streptavidincoated magnetic beads. Anti-CD56 was used to isolate NK cells as

A) Development of the CellMag-CARWash device for single cell isolation



B) Examining single cell EV secretion profiles in droplets using fluorescent imaging

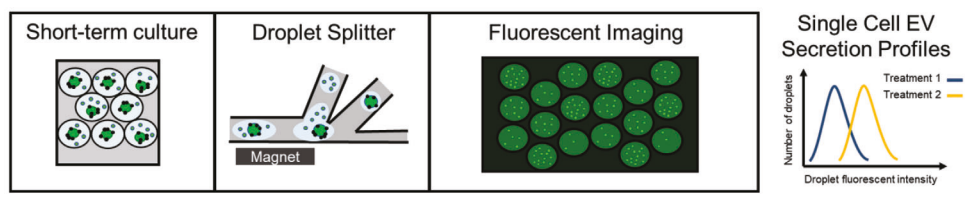


Figure 1. Process Overview. A) Development of the CellMag-CARWash device for single cell isolation. Cells are incubated with 2.8 µm Dynabeads coated with cell type specific antibodies. After incubation with the cells, Dynabeads attach to the desired cell population. The cell mixture is then emulsified into droplets and inputted into the CellMag-CARWash to separate cells attached to Dynabeads into droplets containing a single cell. New media and other cell culture reagents can be used as a wash buffer and added to the new resegmented droplets. B) Examining single cell EV secretion profiles in droplets using fluorescent imaging. Cells in droplets are incubated to allow for single cell EV secretion. After short-term culture, droplets are inputted into a droplet splitter device to divide each droplet into two smaller droplets, one containing the cell and another containing EVs. Droplets containing EVs are placed into a 50 µm tall chamber and imaged. Fluorescence intensity of the droplets is recorded and used to determine relative EV concentration inside the droplets.

CD56 is a known NK cell-surface marker. First, a ratio of 1:2 antibody solution:bead solution, by volume, was incubated for 30 minutes to attach biotinylated antibodies to streptavidin-coated beads before unbound antibodies were washed away. This was followed by a 30-minute incubation of cells and antibody-coated beads which was found to result in beads attached to \approx 90% of all NK cells. Figure 2Ai shows representative images of a mixture of NK (red) and T cells (blue) after incubation with Dynabeads. The Dynabeads attached specifically to NK cells and have minimal attachment to T cells. The number of Dynabeads attached to each cell was determined using brightfield imaging. The distribution of the number of beads per cell is shown in Figure 2Aii (NK cells) and Figure 2Aiii (T cells). Anti-CD56 coated Dynabeads show variable attachment to NK cells, with ≈10% of NK cells having no attached beads and over 10% of cells having ten or more beads attached (average 5.3 beads per cell). Additionally, there was limited nonspecific binding of anti-CD56 beads, as 90% of T cells (CD56 negative cells) showed no attachment to anti-CD56 Dynabeads (average 0.125 beads per cell).

For cancer cell isolation, a mixture of biotinylated anti-Epithelial Cellular Adhesion Molecule (EpCAM), anti-CD133, and anti-EGFR antibodies were added to the Dynabeads on account of heterogeneous expression of surface markers. A ratio of 2:3 antibody solution:bead solution, by volume, with a 1.5-hour incubation of antibody-coated beads with cells was determined to be sufficient for the attachment of Dynabeads to MCF7 GFP cells (Figure 2Bii). After incubation, over 20% of MCF7 GFP cells had 10 or more beads attached, while <5% of cells had less than two beads attached (average 9.8 beads per cell). When mixtures of MCF7 GFP cells and NK cells were introduced to cancer-specific beads, ≈75% of NK cells had less than two beads attached (average 0.51 beads per cell). Mixtures of cells with attached Dynabeads were then input into the CellMag-CARWash device to de-

termine the minimum number of beads per cell needed to recover cells in the product stream.

2.2. Adapting the CellMag-CARWash Device for the Isolation of Cells

Many magnetic cell isolation techniques rely on serial, in-tube wash steps to remove contaminant cell types from the sample. These manual wash steps introduce cell loss and opportunities for interactions between single cells prior to segmentation. Therefore, we designed the CellMag-CARWash device: a new CAR-Wash design optimized for single cell isolation (Figure 3A). The CellMag-CARWash device allows for rapid, complete washing of samples and isolation of desired, magnetic bead-tagged cells. Cells pass through the device on the order of milliseconds and molecular treatments can be applied directly into droplets containing isolated, single cells. This feature eliminates the possibility that extracellular materials such as RNA fragments, EVs, or metabolites could be exchanged between single cells following treatment.

The main design change incorporated since the previous iteration was the lengthening of the magnetophoretic separation chamber. This change was included to account for two potential challenges in recovering cells from the device. First, we anticipated that magnetic bead-tagged cells would experience an increased drag force compared to the previously isolated 10 µm beads with protein, due to Stokes law. Stokes law describes the drag force on small particles in dense solutions, such as media, and states that the drag force is proportional to the object's radius.^[37] Therefore, as bead-tagged cells would be >10 μm, they will experience more resistance to moving toward the magnet and the product stream, reducing recoveries. Second, the smaller

27010198, 2024, 7, Downloaded from https://onlinelibrary.wiley.com/doi/10.1002/adb.202400066, Wiley Online Library on [05/09/2024]. See the Terms and Conditions (https://onlinelibrary.wiley.com/terms-and-conditions) on Wiley Online Library for rules of use; OA articles are governed by the applicable Creative Commons License

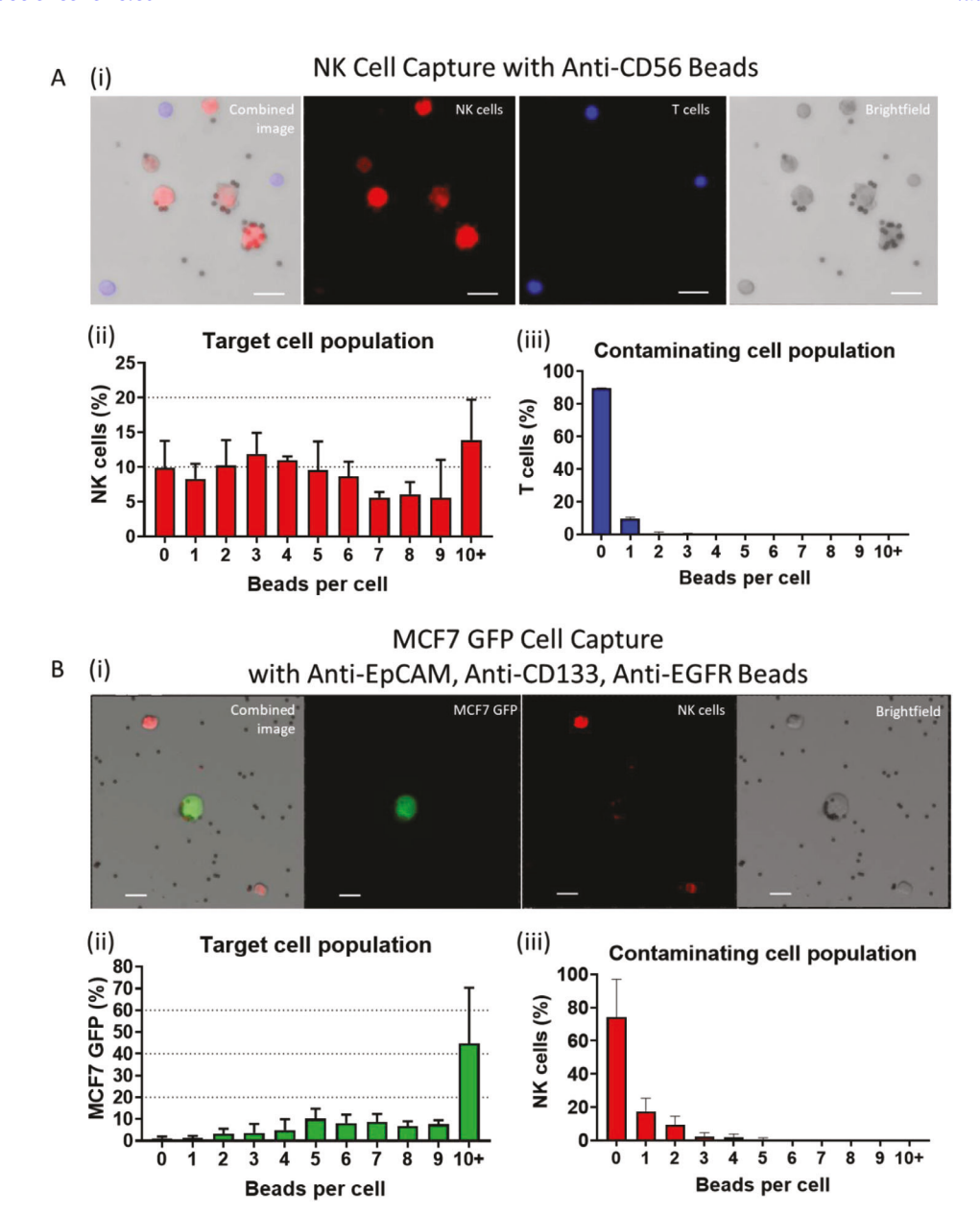


Figure 2. Attachment of 2.8 μm Dynabeads to a desired cell population within a mixed cell population. A) Anti-CD56 coated Dynabeads attached to NK cells in a mixture of NK cells and T cells. i) Images of Dynabeads attached to NK cells (red). T cells are shown in blue. Scale bars indicate 20 μm. ii) Percentage of NK cells with various amounts of anti-CD56 Dynabeads. N = 3 iii) Percentage of T cells with various amounts of anti-CD56 coated Dynabeads. N = 3 B) Anti-EpCAM/ anti-EGFR/ anti-CD133 coated Dynabeads attached to MCF7 GFP cells in a mixture of MCF7 GFP cells and NK cells. i) Images of Dynabeads attached to MCF7 GFP cells (green). Scale bars indicate 20 μm. ii) Percentage of MCF7 GFP cell population with various amounts of anti-EpCAM/ anti-EGFR/ anti-CD133 coated Dynabeads. N = 4 iii) Percentage of NK cell population with various amounts of anti-EpCAM/ anti-EGFR/ anti-CD133 coated Dynabeads. N = 4.

size of the Dynabeads ($2.8~\mu m$ in our system) versus the $10~\mu m$ streptavidin beads would result in a smaller applied magnetic force. Correspondingly, the smaller beads would not be drawn as rapidly to the magnet and thus the bottom of the isolation channel. Extension of the magnetophoretic chamber lengthens the residence time bead-tagged cells spend inside the device, which allows them to further traverse across the washing buffer streamline, toward the magnet. Alternatively, increasing the magnetic field strength applied to the beads could divert Dynabead-tagged cells more rapidly to the product output streamline, demonstrat-

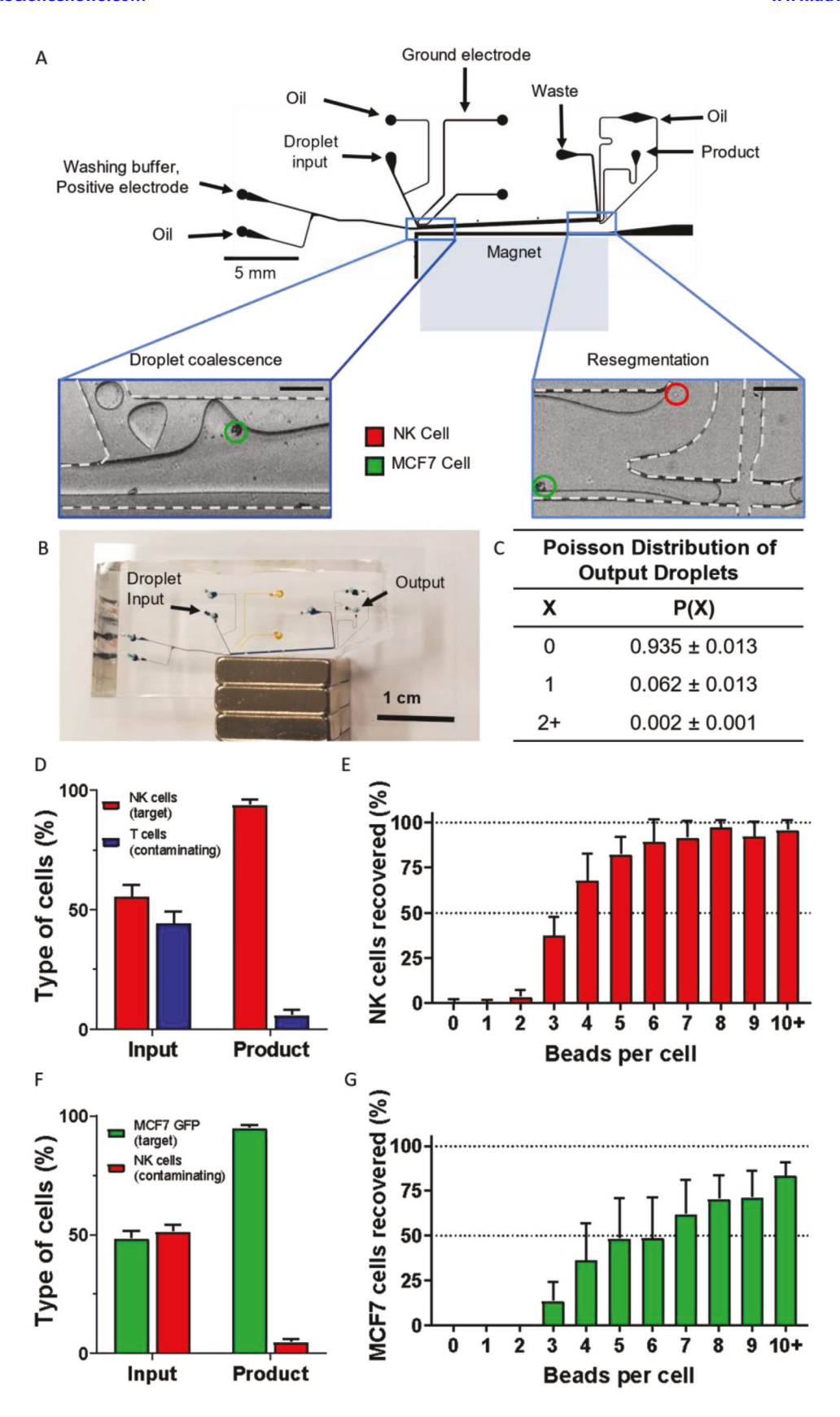
ing the versatility in the users' ability to adapt the system for their application. However, this was not investigated in this study. The balance of these parameters has been discussed in greater detail previously.^[34]

2.3. CellMag-CARWash Processing of Cell Mixtures

Magnetic bead-tagged cells were emulsified into \approx 200 pL sized droplets by flowing the aqueous cell solution and an immiscible

27010198, 2024, 7, Downloaded from https://onlinelbrary.wiley.com/doi/10.1002/adbl.202400066, Wiley Online Library on [05/09/2024]. See the Terms and Conditions (https://onlinelibrary.wiley.com/terms-and-conditions) on Wiley Online Library for rules of use; OA articles are governed by the applicable Creative Commons License

www.advancedsciencenews.com





www.advancedsciencenews.com

ADVANCED BIOLOGY

www.advanced-bio.com

oil phase through a flow focusing droplet generator (Figure S1, Supporting Information). Droplet samples were subsequently loaded and processed through the CellMag-CARWash device to isolate cells of interest (NK cells and MCF7 GFP cells, respectively) into resegmented droplets. Coalescence of initial droplet samples into a wash buffer can be seen in Figure 3A and in Video S1 (Supporting Information). Resegmentation of cells with Dynabeads into new droplets is also shown in Figure 3A and Video S2 (Supporting Information). The actual device is shown in Figure 3B. We estimate that 6% of the droplets exiting the CellMag-CARWash device will contain a single cell according to Poisson distribution (Figure 3C). Fluorescent images of cells in droplets following microfluidic device operation are shown in Figure S2 (Supporting Information). Initial mixtures containing approximately equal amounts of the desired cell type and a contaminating cell type were processed through the CellMag-CARWash. The respective output product streams were enriched for the desired cell type, achieving over 93% and 95% purity for the NK cells and MCF7 GFP cells, respectively (Figure 3D,F).

To determine the number of attached beads needed to recover cells in the product stream, the resulting output droplets and waste streams were separately collected, imaged, and analyzed. Figure 3E,G show the percentage of cells recovered in the product stream based on the number of beads attached, where percentage of cell recovered is defined as:

% of cells recovered

$$= \left(\frac{\text{\# of cells in product stream (droplets)}}{\text{\# of cells in product stream}}\right)$$

$$* 100$$
(1)

It was found that a minimum of four attached beads was needed to recover over half of the NK cells, with near 100% recovery of NK cells achieved when six or more beads were attached. A minimum of five beads was needed to recover over half of the MCF7 GFP cells and a maximum recovery of 83% was achieved when ten or more beads were attached to a cell. We attribute the higher number of beads required to recover the MCF7 GFP cells to their larger size (Figure S3, Supporting Information), which increases the amount of drag forces they experience when traveling across the streamlines of the CellMag-CARWash device.

2.4. Optimizing a Magnetic Droplet Splitter Device to Collect EVs from Droplets Containing Cells

To study EV secretion from cells, we used fluorescent cells capable of secreting fluorescent EVs that could then be imaged via fluorescent microscopy. However, due to size differences between cells and EVs (µm vs nm diameters, respectively), the fluorescent intensity of the cell would be much greater than that from EVs contained within the same droplet. Therefore, it was necessary to incorporate a second device capable of separating cells from EVs. Droplet splitters have previously been used to divide droplets with desired cargo and enrich droplets with sample-bound magnetic beads. [38,39] Our droplet splitter device processed inputted droplets, which after an overnight incubation contained both cells and secreted EVs, and generated two separate output droplets—one containing the cell and another the EVs. After successful EV isolation, secretion could be quantitatively assessed.

Figure 4A shows the device junction where cell-containing droplets were split. Bead-tagged MCF7 GFP cells were attracted to the magnet on device and encapsulated inside the droplets headed to the magnetic output, while EVs in solution passed into both resulting droplets, the cell-containing droplet and a second droplet directed to the EV outlet collection port. Cells can be seen entering the magnetic output as droplets are split in Video S3 (Supporting Information) and the actual device can be seen in Figure 4B. For each experiment, droplets were collected from both the magnetic and EV output, coalesced, and imaged for cells. Figure 4C shows the percentage of cells recovered from the magnetic (cell) output under different parameter conditions, including high or low droplet velocities, and various carrier phases (oils). Lower velocities appeared to have a higher percentage of cells recovered in the magnetic outlet, therefore, sample processing was performed at lower velocities in future experiments. The two carrier phases tested were 2% w/w fluorosurfactant-008 (F008, a fluorinated surfactant used to stabilize droplet-influorinated-oil emulsions) in Novec 7500 oil (N-7500) and fluoroinert FC-40 oil (FC-40). We tested these two carrier phases to assess whether interfacial tension affects cell recovery in the magnetic outlet via the consistency of droplet splitting. Empirically, we found that 2% F008 in Novec 7500 oil compared to FC-40 did not show a statistically significant difference in cell recovery (87.3% vs 86.3%). Two percent F008 in Novec 7500 was chosen for sample processing since its lower interfacial tension could help stabilize droplets after they exited the splitting device, preventing discreet droplets from merging together prior to fluorescence imaging.

Figure 3. CellMag-CARWash cell recovery. A) Diagram of the CellMag-CARWash with labeled input and output streams. The Droplet Coalescence box shows premade droplets containing cells coalescing with the wash buffer upon entering the device. Cells with beads will be attracted to the magnet and resegmentation of droplets containing media (Resegmentation box, bottom right). Cells without beads and other waste components will exit into the waste stream (Resegmentation box, top right). MCF7 GFP cells (target cells) are circled in green. NK cells (contaminating cells) are circled in red. Scale bars indicate 100 μ m, unless otherwise noted. B) Image of the actual device with the droplet input and output labeled. C) Estimated single-cell encapsulation (X = 1) probability (P(X)) for CellMag-CAR-Wash output according to Poisson statistics. X is the number of cells expected in a droplet; P(X) is the probability that X cells would be found in one droplet. D) The percentage of each cell type in the solution, with anti-CD56 beads, inputted into the CellMag-CARWash and recovered from the CellMag-CARWash based on the number of anti-CD56 beads attached to cells. N = 5 F) The percentage of each cell type in the solution, with anti-EpCAM/anti-CD133/anti-EGFR, inputted into the CellMag-CARWash and recovered from the CellMag-CARWash in the product stream. N = 6 G) The percentage of MCF7 GFP cells resegmented and recovered from the CellMag-CARWash based on the number of anti-EpCAM/anti-CD133/anti-EGFR Dynabeads attached to cells. N = 6.

27010198, 2024, 7, Downloaded from https://onlinelibrary.wiley.com/doi/10.1002/adbi.202400066, Wiley Online Library on [05/09/2024]. See the Terms and Conditions (https://onlinelibrary.wiley.com/terms-and-conditions) on Wiley Online Library for rules of use; OA articles are governed by the applicable Creative Commons License

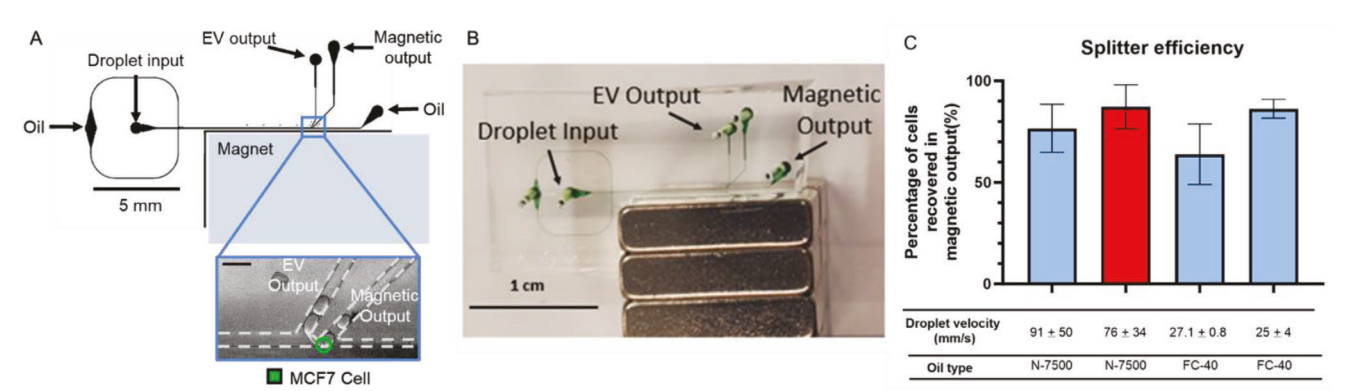


Figure 4. Droplet splitter recovery. A) Diagram of the droplet splitter device. Box shows the junction of the device where droplets are divided into two smaller droplets, with the cell being recovered in the magnetic output. Scale bar indicates $100 \, \mu m$ for inset. B) Image of the actual droplet splitter device with select inputs and outputs identified. C) Recovery of beaded MCF7 GFP cells in the magnetic output based on droplet velocity in the device and they type of oil used, either FC-40 or 2% F008 in N-7500. N = 3. The red bar indicates the condition that was used for future experiments.

To confirm that our workflow would not affect EV secretion, we cultured NK cells in bulk with or without beads attached and collected the secreted EVs, which were isolated from cell culture supernatant using ultracentrifugation. Nanoparticle tracking analysis (NTA) of the collected EV secretions showed relatively consistent concentrations and size distributions (Figure S4, Supporting Information) across both conditions. This suggests that bead attachment does not affect EV secretion.

2.5. Single Cell EV Quantification in Droplets

MCF7 GFP is an estrogen receptor positive cell line, and β -Estradiol has been previously shown to induce the proliferation of these cells. [40] However, the effect of β -Estradiol on MCF7 cell EV secretion has not been studied. Using the CellMag-CARWash cell isolation module and droplet splitting device, we sought to probe MCF7 EV secretion at the single cell level. We first isolated MCF7 GFP cells from a mixture of MCF7 GFP and NK cells, and then placed them into droplets with or without supplemental β -Estradiol in culture media (Dulbecco's Modified Eagle Medium (DMEM)) using the CellMag-CARWash device. Next, after shortterm incubation, we split these droplets to obtain droplets containing fluorescent EVs secreted from single MCF7 GFP cells for fluorescent imaging (Figure 5A). The mean fluorescent intensity of each droplet was measured to reflect the relative EV concentration, with higher fluorescent intensity indicating more EVs within a droplet.

Figure 5B shows the distribution of the fluorescence intensity of multiple droplets generated during a single experiment. Given the high throughput nature of the device, 100s-1000s of droplets were generated and collected for each condition, and this experiment was repeated in triplicate (Figure S5, Supporting Information). The distribution of the fluorescent intensity appeared to be mostly Gaussian with a slight skew to the right for cells cultured without β -Estradiol (Figure 5B). Notably, cells cultured in the presence of 1 μ m β -Estradiol generally showed an increase in fluorescence intensity. This indicates that EV secretion increases upon exposure to β -Estradiol. Interestingly, the distribution of fluorescence intensities observed for β -Estradiol-treated

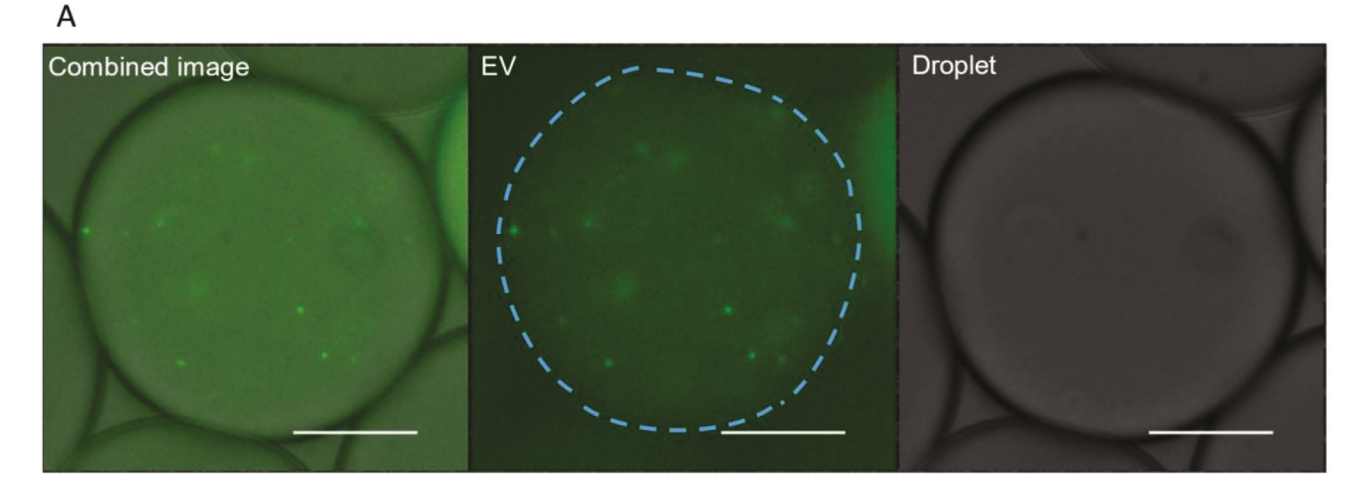
cells appeared broader compared to untreated cells (Figure 5B,C). This finding was consistent when the interquartile was calculated, which removes droplets on the lower and outer ranges that may have either not originally had cells, or had debris causing increased fluorescent signal. These results suggest that the response of this cell line to β -Estradiol is heterogeneous, with some cells being more responsive in their EV secretion than others. When the percentage of cells above the 50% percentile of the DMEM control was calculated, it was found to range from 78% to 90%, while the percentage above the 75% percentile ranged from 54% to 83%. This demonstrates that while the majority of treated cells had higher secretions, some cells did not respond to β -Estradiol.

As EV studies are typically performed in bulk samples, we compared our single cell data to data obtained from bulk cells using traditional methods of isolation and analysis. For bulk MCF7 GFP EV isolation, the supernatant was collected from cells $(\approx 3 \times 10^6 \text{ cells per condition})$ after culturing in DMEM with and without β -Estradiol. EVs were then isolated from the supernatant by ultracentrifugation, before quantification using NTA (see Figure S6, Supporting Information). Figure 5D shows a 2.1fold increase in the relative EV concentration when cells were cultured with 1 μ M β -Estradiol compared to when no β -Estradiol was added. We compared these results to the single cell data by averaging the mean fluorescent intensity of all droplets from three runs (Figure 5E). This showed a 1.8-fold increase in EV secretion from single cells in the presence of 1 $\mu M \beta$ -Estradiol, which was similar to the results obtained from bulk cells. However, as shown above, the single cell measurements reveal heterogeneity in secretion obviated by bulk measurements.

3. Discussion

In this study, we presented a high throughput, droplet microfluidic device, the new CellMag-CARWash, for the specific isolation of single cells from mixtures. By using antibodies that target antigens on the surface of the desired cell population, we were able to isolate cells of interest from a mixed cell population and encapsulate the cells within droplets to study them at a single cell level. We further examined the heterogeneity of single cell EV

27010198, 2024, 7, Downloaded from https://onlinelibrary.wiley.com/doi/10.1002/adb.202400066, Wiley Online Library on [05/09/2024]. See the Terms and Conditions (https://onlinelibrary.wiley.com/terms-and-conditions) on Wiley Online Library for rules of use; OA articles are governed by the applicable Creative Commons License



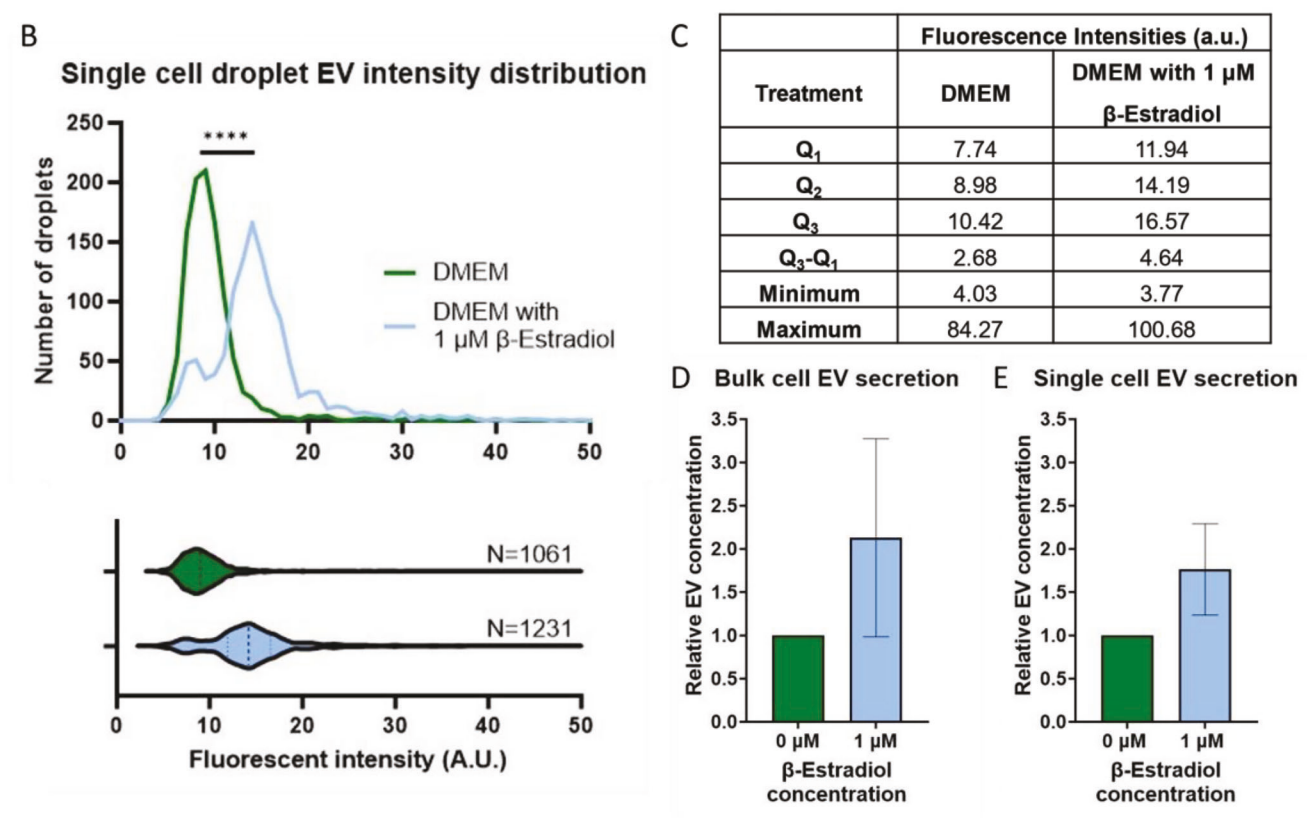


Figure 5. MCF7 GFP EV secretion with various concentrations of β-Estradiol. A) Image of droplet with fluorescent EVs taken at 60X magnification. Dotted line indicates droplet border. Scale bar indicates 20 μm. B) Distribution of fluorescent intensities of droplets containing EVs secreted by single cells. P value <0.0001. C) Statistical landmarks of the single cell fluorescence intensity dataset. Quartile regions, the range between the first and third quartiles, the minimum, and the maximum are included for both single cell treatments. D) Relative EV concentration obtained from the supernatant of bulk MCF7 GFP cells cultured with various concentrations of β-Estradiol. N = 3 E) Relative EV concentration of EVs secreted by single cell based on the mean fluorescent intensity of the droplets post droplet splitter, compared to the background fluorescent intensity. Experiments performed in triplicate.

secretions by culturing individual cells in droplets short-term to allow for EV secretion before imaging and analysis. This analysis showed differences in the EV secretion profiles within cells from the same population that were exposed to different media components.

First, to demonstrate the cell recovery of the CellMag-CARWash device, we calculated the percent recovery of two differ-

ent cell populations, NK cells, and MCF7 GFP cells, based on the number of antibody-coated magnetic beads that were attached to the cells. Over half of NK cells processed through the device were recovered when there were four beads attached to the cells. The recovery increased as more beads were attached, with >90% of cells recovered when six or more beads were attached. However, MCF7 GFP cells required a minimum of five attached beads to

SCIENCE NEWS

www.advancedsciencenews.com

achieve a 50% recovery in the device, and the maximum recovery was limited to 83% with ten or more beads attached. As the MCF7 GFP cells used in these experiments were, on average, 8.3 um larger in diameter compared to NK cells (Figure \$3, Supporting Information), we believe the different performance is due to the cell size and the corresponding increase in drag force. Further, lengthening of the CellMag-CARWash magnetophoretic chamber, increasing the magnetic field strength, or reducing the velocity to allow cells more time to be attracted to the product stream could further improve recoveries. However, these changes would allow cells with fewer beads attached to enter the product stream, and due to nonspecific binding of beads to the contaminating cell population, we expect this would result in a decrease in purity. Currently, three or more beads per cell are needed to recover cells from the device. As only 0.27% and 4.51% of contaminating cells have three or more beads attached when using anti-CD56 coated beads and anti-EpCAM/ anti-CD133/ anti-EGFR coated beads respectively, we are able to achieve a purity of over 93% with the current parameters. Additionally, modulation of the magnetic field strength applied by the magnets would enable the user to control the balance of recovery rates and output purity as desired without making changes to the device design in future iterations. Future users may choose to modify these features—magnetophoretic chamber length, magnetic field strength, and fluid velocity—to tune the CellMag-CARWash to isolate cells with varying levels of antigen expression or size.

After processing cells with the CellMag-CARWash device, cells were incubated in droplets short-term to allow for EVs to be secreted before being processed through a magnetic droplet splitter. The droplet splitter was designed to separate fluorescent cells from droplets with EVs to reduce the fluorescent background and improve EV quantification. Operational conditions tested in this device were 1) velocity of droplets in the device and 2) type of oil used for emulsion. The magnet was positioned below the junction, to attract cells toward the bottom of the droplet, where they are positioned to flow into the magnetic outlet. We found that slower velocities improved the recovery of cells into the magnetic output, suggesting that at lower speeds the cells had more time to move into the correct position within the droplet, or that internal vortices present in the droplet were reduced, stabilizing the cell's position inside the droplet. The two oils tested had different interfacial tensions, which we hypothesized may affect the likelihood of the droplet to split, as failure to split could result in cells exiting the wrong output. However, this appeared to have little difference in the overall recoveries, suggesting that droplets were consistently splitting in both oil phases.

To validate the whole system, a mixture of MCF7 GFP cells and NK cells with magnetic beads specifically attached to the MCF7 GFP cells was inputted into the CellMag-CARWash, placed into droplets, incubated for 18 hours, and split using the droplet splitter before imaging of droplets with EVs. The cells were kept in either DMEM or DMEM with β -Estradiol, which was added via the wash buffer during CellMag-CARWash processing. The mean single cell EV secretion in droplets, measured by the fluorescent intensity of the droplets, was compared to bulk cell EV secretion obtained from ultracentrifugation and NTA analysis. Both methods showed a similar increase in EV concentration when β -Estradiol was added, indicating that we observed the same stimulation phenomenon regardless of the isolation and quantification methods used. However, the profiling of single droplets provided additional insight into the variation in cells response to β -Estradiol that can not be observed via bulk analysis. For example, we were able to observe a range of fluorescence intensities in resulting droplets and consequently, a range in the level of EV secretion produced from both DMEM- and DMEM with β -Estradioltreated cells, indicating natural heterogeneity in EV secretion levels for the cell line. By calculating the interquartile range of fluorescent intensity, we observed that the range of the distribution was consistently broader for β -Estradiol-treated cells, indicating that MCF7 GFP cells responded heterogeneously to the stimulation. The interquartile range was used as it eliminates droplets on either end of the distribution, including those that may be empty or contain fluorescent debris. To decrease the number of empty droplets, post-encapsulation sorting could be added to collect only droplets containing a cell.[41] Additionally, imaging and analysis could be improved to enable the processing of droplets that contain cells and EVs. This would eliminate the need for a droplet splitter and allow users to see the original cell that the EVs originated from. A workflow to perform this analysis has been previously reported by Hattori et al., [36] but lacks the pre-sorting of specific cell populations that the CellMag-CARWash offers.

www.advanced-bio.com

The CellMag-CARWash device offered several additional advantages for single cell work due to the buffer exchange design. Passing cells through a wash buffer before their resegmentation into droplets allows for both the removal of other cell populations and waste components, and can introduce new reagents to the cells necessary for downstream applications. The washing design is especially beneficial for solutions such as blood, which have multiple cell types and components, such as platelets, that complicate further analysis. Buffers used in the device are interchangeable, provided the solution has an ionic charge, so that it can function as the positive electrode in the device. Therefore, multiple different buffers could be used in the device for a broad range of downstream applications. While this workflow was used to examine the profile of single cell EV secretions, we believe that the CellMag-CARWash device could be a useful tool for streamlining and improving alternative single cell studies. As the magnetic beads used in this work were streptavidin-coated, the application and desired target cell population recovered can be changed by the user by adjusting the biotinylated antibodies used. In cases where cell surface expression may be variable, multiple antibodies can be added to beads to improve attachment. For alternative downstream assays, future users may choose to link the CellMag-CARWash to additional processing devices, [42,43] or alter the design to add in components for cell lysis, reverse transcription, PCR, and/or sample barcoding to perform single cell transcriptomic and epigenomic analyses. [3,32,33,44] The product droplets also compartmentalize secreted components along with single cells, as shown, so analysis could be expanded to other secreted molecules like cytokines or metabolites.[2,45]

In conclusion, the CellMag-CARWash device offers fast, specific isolation and encapsulation of a target cell population for single cell studies. By performing the isolation of cells on device before encapsulation, researchers can quickly pre-select cells of interest for downstream analysis. Once generated, each droplet can be individually assayed to observe unique differences in cell behavior. While multiple downstream assays can be performed on single cell droplets, we used the generated droplets to observe



SCIENCE NEWS

www.advancedsciencenews.com

ADVANCED BIOLOGY

www.advanced-bio.com

differences in the secretion of EVs from cells from the same population, and observed a heterogeneous increase in MCF7 GFP EV secretion in the presence of β -Estradiol. The observation of these data features that can only be observed at the single cell level merits further development of integrated technologies that advance studies on single cell EV secretion.

4. Experimental Section

Cell Culture: Cell stocks were purchased from ATCC. All cell lines were cultured at 37 °C, 5% CO₂ under normoxic conditions. NK92mi cells were cultured in a T75 flask with minimum essential medium alpha (10 mL, MEM-a, Thermo Fisher, Cat# 12561056) supplemented with 10% fetal bovine serum (Sigma, Cat# F2442), 10% horse serum (Thermo Fisher, Cat# 16050122), 0.1% myo-inositol (Sigma, Cat# 17508), 0.1% folic acid (Sigma, Cat# F8758) and 1% antibiotic-antimycotic (Thermo Fisher, Cat# 15240062). Jurkat cells (T cells) were cultured in a T75 flask with Roswell Park Memorial Institute (10 mL, RPMI, Thermo Fisher, Cat# 11875093) supplemented with 10% fetal bovine serum and 1% antibiotic-antimycotic. MCF7 GFP cells were cultured in a T75 flask with Dulbecco's Modified Eagle's Medium (10 mL, DMEM, Thermo Fisher, Cat# 11995065) supplemented with 10% fetal bovine serum and 1% antibiotic-antimycotic. NK92mi cells and Jurkat cells were subcultured every 2-3 days by removing 80-90% of the cell solution and replacing it with fresh media. MCF7 GFP cells were subcultured when they reached 70-80% using Tryp-LE (Thermo Fisher, Cat# 12604013). All cell lines were tested and reported negative for mycoplasma using MycoAlert Mycoplasma Detection Kit (Lonza, Cat# LT07-703).

To better visualize cells and improve the analysis, NK cells and T cells were fluorescently labeled with CellTracker dye (Thermo Fisher, Cat# C7025, C34565). Cells were removed from culture, washed with PBS to ensure no serum remained, and resuspended in serum free media (5 mL) with CellTracker (5 μ L). The cells were incubated for 30 minutes at 37 °C before being washed twice with PBS to remove the remaining CellTracker.

Magnetic Bead Preparation and Attachment to Cells: To isolate cells using magnetic beads, cell-specific antibodies were first conjugated onto magnetic beads before attaching the beads to the cells. First, the streptavidin-coated M280, 2.8 µm Dynabeads (Thermo Fisher, Cat# 11205D) were removed from the sterile bottle and rinsed 5x with 0.2 µm filtered PBS by pressing a magnet to the side of the tube, allowing the liquid to be removed and the beads left behind. The clean beads were then resuspended in their original volume of 0.1% BSA (Sigma, Cat# A9418) in PBS. For NK cell attachment, biotinylated anti-CD56 antibodies (R&D Systems, cat# BAF2408) were then incubated with the beads at room temperature for 30 min on a rocker, allowing the biotinylated antibodies to bind with the streptavidin-coated Dynabeads. For MCF7 GFP cell attachment, biotinylated anti-EpCAM (R&D Systems, Cat# BAF960), anti-CD133 (Miltenyi Biotec, Cat# 130-113-185), and anti-EGFR (RayBiotech, Cat# MD-02-0006) antibodies were incubated with beads. Following antibody binding, the excess antibody was rinsed off by diluting the bead-antibody solution with 0.1% BSA in PBS (1 mL). The beads were then again trapped using a magnet, allowing the solution to be removed. The conjugated beads were rinsed four times. After conjugation, beads were incubated with the cells of interest at room temperature on the rocker for either 30 min (NK cell attachment) or 1.5 h (MCF7 GFP attachment). Before further experimentation, bead-tagged cells were imaged to ensure effective bead attachment.

Microfluidic Device Fabrication: Device fabrication has been described previously. [34] Masters were fabricated using standard photolithography techniques. SU-8 2025 negative epoxy photoresist was spin coated to a thickness of \approx 40 μm on a silicon wafer and baked. It was exposed to UV light through a design mask transparency obtained from CAD/Art Services, Inc. Device designs were constructed using AutoCAD software. Unpolymerized photoresist was removed via development in propylene glycol monomethyl ether acetate. After baking, wafers were treated with tridecafluoro-1,1,2,2-tetrahydrooctyl trichlorosilane using chemical vapor deposition. To fabricate devices, polydimethylsiloxane (PDMS) was mixed at a 10:1 ratio of base to curing agent, degassed, and poured onto the master. Once cured, the PDMS stamp was cut out and ports were punched out using a 30-gauge needle or a 0.75 mm biopsy punch (Robbins Instruments, Cat# RBP-075). The stamp was bonded to a glass slide (droplet generation) or coverslip (CellMag-CARWash) via oxygen plasma activa-

Microfluidic Device Set-Up: All devices were treated prior to the experiment with aquapel (Pittsburg Glass Works, Cat# 47100); this incubated for one minute before being flushed and replaced with FC-40 oil (Sigma Aldrich, Cat# F9755). Pieces of #30 PTFE Masterflex tubing (Masterflex, Cat# 06417-11) were inserted into the device ports and then their respective pressure vial. The output tubing of each device was collected into a 0.6 mL Eppendorf tube. 1% (w/v) Fluorosurfactant-008 (RAN Biotechnologies, Inc, 008-FluoroSurfactant-1G; abbreviated F008) in Novec 7500 oil (The 3M Company; Novec 7500) which served as the oil phase for droplet generation and CellMag-CARWash processing.

Reagents were delivered on device using a custom-built pressure controller. Nitrogen gas was directed into two splitting manifolds that connect to several two-stage regulators. These regulators allow for pressure selection. The gas then passed through an array of LHDA0531115H solenoid valves that actuate in response to LabView signals from an NI PCIE-6251 multifunction data acquisition device. The headspaces of reagent vials were pressurized via steel pins, and reagent was driven onto the devices via 20 cm long pieces of #30 PTFE tubing. Both droplet generation and CellMag-CARWash devices were imaged on a Leica Dmi8 light microscope, and videos were captured using a VEO 640L high-speed camera from Vision Research Inc. Image processing occurs using ImageJ software from the National Institute of Health (NIH).

Single Cell Droplet Generation: Doonan et al. has previously described the general droplet generation process, [34] thus, here the specifications for this system are described. The cell solution was pipetted to mix the contents before $30-50\,\mu\text{L}$ was aspirated to load into the "sample hopper". The hopper consists of a cut 200 µL pipette tip placed inside a pressure vial and connected to the device via 5 cm length of #30 PTFE tubing and 5 mm length of Tygon tubing (Masterflex, Cat# 06460-18). This vial was inverted to contain the sample inside the pipette tip. Typical pressure settings would be 75 kPa for the oil and 60 kPa for the cell solution.

Device operation took between 5 and 15 min, depending on sample size. At the end of the operation, air entered the device, at which point the cell solution pressure was turned off to allow the oil to rinse the sample hopper. At this point, sample loading and device operation would be repeated. The device can be re-used several times for identical samples. Device usability was determined through brightfield imaging of the device to check for blockages or contamination. Output droplets were rinsed with oil phase before the tube cap was cut off, and the tube was placed inside a vial to be pressurized to deliver droplets onto the following

CellMag-CARWash Processing: Droplets were injected (≈35 kPa) into the device and initially spaced out with an oil spacer (≈45 kPa). Droplets entered the washing chamber and were coalesced with the wash buffer (≈45 kPa) due to application of an electric field. The electric field was delivered via a ground electrode channel filled with 3 M sodium chloride. A platinum wire was inserted into the wash buffer solution to serve as the positive electrode. After coalescence, cells were carried along by the washing buffer. Magnetic-bead-tagged cells were attracted toward the eight Neodymium magnets installed on the device, ≈400 μm away from the washing channel. An oil co-flow (≈45 kPa) was used to prevent cells and magnetic beads from sticking to the channel walls. Cells and magnetic beads in the lowest streamline were resegmented into new droplets at the end of the device. All other materials in the buffer stream were sent into waste (≈15 kPa). The sizing of output droplets could be adjusted by varying the pressure of a 2% (w/v) F008 in Novec 7500 oil phase input (≈30 kPa) at the resegmenting junction. Output droplets could be collected for imaging analysis or sent to downstream processing steps at this point. For future magnetic droplet splitting, droplets were collected into a 12-well plate and incubated overnight at 37 °C. An extra oil phase was added as necessary to keep droplets hydrated, and prevent breakage

www.advancedsciencenews.com

ADVANCED BIOLOGY

www.advanced-bio.com

Operation time typically takes between 15 and 45 min, depending on sample size. Wash buffer and the oil phases were used to rinse the sample input tubing and carry all resegmented droplets into the collection. Each CellMag-CARWash device could be reused for replicate samples, but a new device was set up for different sample types or in response to debris collecting within the channel.

Magnetic Droplet Splitter Processing: Following overnight incubation, samples were collected into Eppendorf tubes and prepared for processing on a magnetic droplet splitting device as they were prior to processing via CellMag-CARWash. On device, droplets ($\approx\!30~\text{kPa}$) were spaced out by an oil flow ($\approx\!25~\text{kPa};~2\%$ (w/v) F008 in Novec 7500 oil) before traveling through a channel lined by eight Neodymium magnets installed in the coverslip and encountering a channel wall that juts into the channel. Droplet volume then split into two output channels, with magnetic bead-tagged cells entering the right-most output, due to their attraction to the lower channel wall. One of the output channels was contained in a vial that can be pressurized to assist with troubleshooting fibers stuck in the device. A second oil flow ($\approx\!20~\text{kPa};~2\%$ (w/v) F008 in Novec 7500 oil) was applied at the splitting junction to enable real-time adjustment of the volumes sent into each output channel.

Droplet Manipulation and Analysis Coalescence: Following droplet generation, CellMag-CARWash processing, and/or magnetic droplet splitting, cells in droplets (referred to as simply droplets) were either kept intact to investigate droplet stability and cell viability in live cell experiments, or coalesced using 1H,1H,2H,2H-perfluoro-1-octanol (Sigma Aldrich, Cat# 370533) to gather the cells into the aqueous phase for ease of counting.

Droplets were combined via coalescence to form one aqueous phase that can be distinguished as a layer on top of the oil phase. The aqueous phase with cells was removed and put into a well plate for imaging. Droplets were coalesced from the CellMag-CARWash product and waste streams, as well as from the droplet splitter EV and magnetic outputs. After coalescence, cells were imaged at 30x in fluorescent channels to identify cell types and quantities, and in brightfield to quantify the number of beads per cell using a Nikon Ti2 Eclipse microscope.

Bulk EV Quantification Using Nanoparticle Tracking Analysis (NTA): NTA for EVs secreted from cells with and without beads (Figure S4, Supporting Information) was performed using the Malvern NanoSight system. A diluted EV solution obtained from ultracentrifugation was injected into the machine to obtain five 60-second-long videos of EVs in scatter mode. Data acquisition and processing were performed using the NanoSight NS300 control software. For each video, the concentration of the particles in the size range of 30 -1000 nm was determined. The average concentration and particle size for each sample were determined and reported.

NTA for EVs secreted from a bulk solution of cells cultured with and without $\beta\textsc{-Estradiol}$ (Figure 5D; Figure S6, Supporting Information) was performed using the Zetaview (Particle Metrix). A diluted EV solution obtained from ultracentrifugation was injected into the machine, and the concentration and particle size were determined across 11 positions in the chamber. This was repeated three times for each sample. To account for diffusion limitations in the chamber, the average of the three highest concentrations from each replicate was used to determine an overall sample concentration. The concentration was normalized to the original volume and a relative concentration based on samples cultured without $\beta\textsc{-Estradiol}$ was determined.

Single Cell Secreted EV Droplet Analysis: To evaluate the single cell EV concentration in droplets, after processing with the droplet splitter, droplets were placed in the 50 μm tall imaging chamber device. The imaging chamber consisted of the PDMS top that was previously described in Yoon et al, but briefly is a 50 μm tall single chamber that is approximately the dimensions of a 1″x3″ glass slide. $^{[46]}$ The difference in the imaging chamber used here is that the PDMS chamber is bonded using an O_2 plasma etcher directly to a glass slide, creating one large chamber. Imaging chambers were first primed with oil before loading the droplets using a Harvard syringe pump at 10 μL min $^{-1}$. Once droplets were loaded into the chamber, the device was imaged at a 60x objective. Post-imaging analysis was done on the Nikon Elements software. Briefly, 100+ droplets from each sample were manually identified and their border circled. Any droplet

that contained a cell was removed from the analysis. The fluorescent intensity of each circled object was recorded. Additionally, regions with no droplets were identified and circled to obtain the background fluorescent intensity of the device. This average background intensity was subtracted from each droplet to obtain the normalized fluorescent intensity for each droplet.

Supporting Information

Supporting Information is available from the Wiley Online Library or from the author.

Acknowledgements

B.T.R., C.D.C., and E.A.P. contributed equally to this work as co-first authors. The authors gratefully acknowledge the Forbes Institute and the National Science Foundation (Understanding the Rules of Life Epigenetics: 1921677) for financial support for B.T.R. and C.D.C., respectively, to complete this work. E.A.P. and N.M. were supported by the Microfluidics in Biomedical Sciences Training Program. This research was also funded by the National Institute of Health (R01-CA-208335-01-A1 to S.N.), a Lefkofsky Scholar award and Rogel Scholar award to S.N. The authors also thank the Lurie Nanofabrication Facility for access to their microfabrication equipment.

Conflict of Interest

The authors declare no conflict of interest.

Data Availability Statement

The data that support the findings of this study are available from the corresponding author upon reasonable request.

Keywords

droplet microfluidics, extracellular vesicle, magnetic cell isolation, single cell

Received: April 4, 2024 Published online: May 13, 2024

- [1] S. J. Altschuler, L. F. Wu, Cell 2010, 4, 559.
- [2] L. Mazutis, J. Gilbert, W. L. Ung, D. A. Weitz, A. D. Griffiths, J. A. Heyman, Nat. Protoc. 2013, 5, 870.
- [3] E. Z. Macosko, A. Basu, R. Satija, J. Nemesh, K. Shekhar, M. Goldman, I. Tirosh, A. R. Bialas, N. Kamitaki, E. M. Martersteck, J. J. Trombetta, D. A. Weitz, J. R. Sanes, A. K. Shalek, A. Regev, S. A. McCarroll, Cell 2015, 5, 1202.
- [4] P. Shahi, S. C. Kim, J. R. Haliburton, Z. J. Gartner, A. R. Abate, Sci. Rep. 2017, 1, 44447.
- [5] F. Lan, B. Demaree, N. Ahmed, A. R. Abate, *Nat. Biotechnol.* 2017, 7, 640.
- [6] B. Demaree, C. L. Delley, H. N. Vasudevan, C. A. C. Peretz, D. Ruff, C. C. Smith, A. R. Abate, *Nat. Commun.* 2021, 1, 1583.
- [7] Nat. Methods 2014, 11, 1.
- [8] Nat. Methods 2020, 17, 1.

ADVANCED BIOLOGY

www.advancedsciencenews.com

www.advanced-bio.com

- [9] A. A. Alizadeh, V. Aranda, A. Bardelli, C. Blanpain, C. Bock, C. Borowski, C. Caldas, A. Califano, M. Doherty, M. Elsner, M. Esteller, R. Fitzgerald, J. O. Korbel, P. Lichter, C. E. Mason, N. Navin, D. Pe'er, K. Polyak, C. W. M. Roberts, L. Siu, A. Snyder, H. Stower, C. Swanton, R. G. W. Verhaak, J. C. Zenklusen, J. Zuber, J. Zucman-Rossi, Nat. Med. 2015, 8, 846.
- [10] E. Papalexi, R. Satija, Nat. Rev. Immunol. 2018, 1, 35.
- [11] C. A. Stewart, C. M. Gay, Y. Xi, S. Sivajothi, V. Sivakamasundari, J. Fujimoto, M. Bolisetty, P. M. Hartsfield, V. Balasubramaniyan, M. D. Chalishazar, C. Moran, N. Kalhor, J. Stewart, H. Tran, S. G. Swisher, J. A. Roth, J. Zhang, J. De Groot, B. Glisson, T. G. Oliver, J. V. Heymach, I. Wistuba, P. Robson, J. Wang, L. A. Byers, Nat. Cancer 2020, 4, 423.
- [12] G. M. Cooper, in The Cell: A Molecular Approach; Sinauer Associates, Sunderland, MA, 2nd ed, 2000.
- [13] L. Gangoda, S. Boukouris, M. Liem, H. Kalra, S. Mathivanan, Proteomics 2015, 2-3, 260.
- [14] P. Simeone, G. Bologna, P. Lanuti, L. Pierdomenico, M. T. Guagnano, D. Pieragostino, P. Del Boccio, D. Vergara, M. Marchisio, S. Miscia, R. Mariani-Costantini, *Int. J. Mol. Sci.* 2020, 7, 2514.
- [15] S. Dechantsreiter, A. R. Ambrose, J. D. Worboys, J. M. E. Lim, S. Liu, R. Shah, M. A. Montero, A. M. Quinn, T. Hussell, G. M. Tannahill, D. M. Davis, J. Extracell Vesicles 2022, 4, e12215.
- [16] K. Radhakrishnan, Á. Halász, D. Vlachos, J. S. Edwards, Curr. Opin. Biotechnol. 2010, 5, 677.
- [17] Y. Zhou, N. Shao, R. Bessa de Castro, P. Zhang, Y. Ma, X. Liu, F. Huang, R.-F. Wang, L. Qin, Cell Rep. 2020, 31, 107574.
- [18] A. A. Almet, Z. Cang, S. Jin, Q. Nie, Curr. Opin. Syst. Biol. 2021, 26,
- [19] G. Eraslan, E. Drokhlyansky, S. Anand, E. Fiskin, A. Subramanian, M. Slyper, J. Wang, N. Van Wittenberghe, J. M. Rouhana, J. Waldman, O. Ashenberg, M. Lek, D. Dionne, T. S. Win, M. S. Cuoco, O. Kuksenko, A. M. Tsankov, P. A. Branton, J. L. Marshall, A. Greka, G. Getz, A. V. Segrè, F. Aguet, O. Rozenblatt-Rosen, K. G. Ardlie, A. Regev, Science 2022, 376, eabl4290..
- [20] S. Srivastava, S. N. Furlan, C. A. Jaeger-Ruckstuhl, M. Sarvothama, C. Berger, K. S. Smythe, S. M. Garrison, J. M. Specht, S. M. Lee, R. A. Amezquita, V. Voillet, V. Muhunthan, S. Yechan-Gunja, S. P. S. Pillai, C. Rader, A. M. Houghton, R. H. Pierce, R. Gottardo, D. G. Maloney, S. R. Riddell, *Cancer Cell* 2021, 2, 193.
- [21] H. Zhang, A. Madi, N. Yosef, N. Chihara, A. Awasthi, C. Pot, C. Lambden, A. Srivastava, P. R. Burkett, J. Nyman, E. Christian, Y. Etminan, A. Lee, H. Stroh, J. Xia, K. Karwacz, P. I. Thakore, N. Acharya, A. Schnell, C. Wang, L. Apetoh, O. Rozenblatt-Rosen, A. C. Anderson, A. Regev, V. K. Kuchroo, Cell Rep. 2020, 8, 108433.
- [22] A. Gross, J. Schoendube, S. Zimmermann, M. Steeb, R. Zengerle, P. Koltay, Int. J. Mol. Sci. 2015, 8, 16897.
- [23] P. Hu, W. Zhang, H. Xin, G. Deng, Front. Cell Dev. Biol. 2016.

- [24] K. Matuła, F. Rivello, W. T. S. Huck, Adv. Biosyst. 2020, 1, 1900188.
- [25] M. Di Trapani, N. Manaresi, G. Medoro, Cytometry, Part A 2018, 12, 1260
- [26] M. A. Unger, H.-P. Chou, T. Thorsen, A. Scherer, S. R. Quake, Science 2000, 5463, 113.
- [27] B. Rupp, S. Owen, H. Ball, K. J. Smith, V. Gunchick, E. T. Keller, V. Sahai, S. Nagrath, *Int. J. Mol. Sci.* 2022, 14, 7852.
- [28] S. Owen, T.-W. Lo, S. Fouladdel, M. Zeinali, E. Keller, E. Azizi, N. Ramnath, S. Nagrath, Adv. Biosyst. 2020, 8, 2000110.
- [29] P. See, J. Lum, J. Chen, F. Ginhoux, Front. Immunol. 2018, 9, 2425.
- [30] Y. Xin, J. Kim, M. Ni, Y. Wei, H. Okamoto, J. Lee, C. Adler, K. Cavino, A. J. Murphy, G. D. Yancopoulos, H. C. Lin, J. Gromada, *Proc. Natl. Acad. Sci. USA* 2016, 12, 3293.
- [31] C. W. Fung, S. N. Chan, A. R. Wu, Biomicrofluidics 2020, 2, 021502.
- [32] F. Tang, C. Barbacioru, Y. Wang, E. Nordman, C. Lee, N. Xu, X. Wang, J. Bodeau, B. B. Tuch, A. Siddiqui, K. Lao, M. A. Surani, *Nat. Methods* 2009, 5, 377.
- [33] A. T. Satpathy, J. M. Granja, K. E. Yost, Y. Qi, F. Meschi, G. P. McDermott, B. N. Olsen, M. R. Mumbach, S. E. Pierce, M. R. Corces, P. Shah, J. C. Bell, D. Jhutty, C. M. Nemec, J. Wang, L. Wang, Y. Yin, P. G. Giresi, A. L. S. Chang, G. X. Y. Zheng, W. J. Greenleaf, H. Y. Chang, Nat. Biotechnol. 2019, 8, 925.
- [34] S. R. Doonan, M. Lin, R. C. Bailey, Lab Chip 2019, 9, 1589.
- [35] Y. Ji, D. Qi, L. Li, H. Su, X. Li, Y. Luo, B. Sun, F. Zhang, B. Lin, T. Liu, Y. Lu, Proc. Natl. Acad. Sci. USA 2019, 13, 5979.
- [36] K. Hattori, Y. Goda, M. Yamashita, Y. Yoshioka, R. Kojima, S. Ota, Anal. Chem. 2022, 32, 11209.
- [37] P. P. Urone, College Physics, OpenStax, Houston, TX 2012
- [38] E. Brouzes, T. Kruse, R. Kimmerling, H. H. Strey, *Lab Chip* **2015**, *3*,
- [39] L. Ménétrier-Deremble, P. Tabeling, Phys. Rev. E 2006, 3, 035303.
- [40] C. H. Wu, H. Y. Chuang, C. L. Wang, C. Y. Long, T. H. Hsieh, E. M. Tsai, Mol. Med. Rep. 2019, 19, 2341.
- [41] D. J. Collins, A. Neild, A. deMello, A.-Q. Liu, Y. Ai, Lab Chip 2015, 17, 3439
- [42] Y. Xu, J.-H. Lee, Z. Li, L. Wang, T. Ordog, R. C. Bailey, Lab Chip 2018, 17, 2583.
- [43] A. Rotem, O. Ram, N. Shoresh, R. A. Sperling, A. Goren, D. A. Weitz, B. E. Bernstein, *Nat. Biotechnol.* 2015, 11, 1165.
- [44] C. A. Lareau, F. M. Duarte, J. G. Chew, V. K. Kartha, Z. D. Burkett, A. S. Kohlway, D. Pokholok, M. J. Aryee, F. J. Steemers, R. Lebofsky, J. D. Buenrostro. *Nat. Biotechnol.* **2019**. *8*. 916.
- [45] S. A. Baker, J. Rutter, Nat. Rev. Mol. Cell Biol. 2023, 5, 355.
- [46] H. J. Yoon, T. H. Kim, Z. Zhang, E. Azizi, T. M. Pham, C. Paoletti, J. Lin, N. Ramnath, M. S. Wicha, D. F. Hayes, D. M. Simeone, S. Nagrath, Nature Nanotech 2019, 8, 735.